

REMOTE SENSING OF AIR-SEA INTERACTION.

David Atlas and Erik Mollo-Christensen
Goddard Laboratory for Atmospheric Sciences
NASA/Goddard Space Flight Center
Greenbelt, Maryland 20771

ABSTRACT

We set out a number of preliminary concepts for the measurement or inference of fluxes across the air-sea interface through remote sensing. All the methods are achievable from aircraft with state-of-the-art technology. Only one is now ready for space implementation. The focus is on cold outbreaks. It is possible to infer sensible (latent) heat flux from the difference between initial surface air temperature (vapor mixing ratio) and the downwind SST (and corresponding saturation mixing ratio). The downwind growth rate of the PBL as measured by lidar also provides estimates of surface heating and the cross-inversion entrainment velocity. The lidar also provides a measure of the depth of the inversion and its penetration by surface-forced convection; this permits estimates of the surface heat flux. Lidar and radiometric measurements of cloud top height and temperature provide means of deducing the temperature sounding downstream so that heating may be computed with the aid of a known sounding upstream. Vapor fluxes are measurable by differencing total precipitable water at two ends of a path measured by either IR or microwave radiometers. All the methods suffer from deficiencies; these are discussed.

1. INTRODUCTION

This work attempts to advance our understanding of possible methods for the measurement or inference of fluxes across the air-sea interface through remote sensing. We are concerned mainly with measurements from space; however, the concepts are generally applicable to aircraft platforms as well. The problem is a difficult one for which there are no straightforward solutions. Much of the work in this realm is therefore of a preliminary nature (Gautier, 1980) or deals with methods which are applicable under restricted conditions (Chou and Atlas, 1982). This paper is an extension of that of Chou and Atlas. It is also a synthesis of relatively recent findings and developments and a variety of untested concepts. Thus, the discussion is speculative.

The bulk of the sensible and latent heat fluxes over the globe occur over the warm western boundary currents during winter. For this reason, we focus on the phenomenon of the cold air outbreak. Indeed, we shall see that flux measurements and inferences are more readily made under such conditions.

2. METHODS OF ESTIMATING SEA SURFACE HEAT AND MOISTURE FLUXES

2.1 Downstream Horizontal Gradients of Surface Properties

We start from the premise that no remote sensing technique can sense potential temperature (θ) or vapor density (q) in the lower few tens of meters of the atmosphere. As a result, it is not possible to use the conventional bulk formulas for the fluxes, such as an expression of the form for the flux of the property x

$$F = uC[x(z) - x(0)] \quad (1)$$

Here, u is the wind speed at "anemometer height" (usually at 10 m), C is a constant transfer coefficient, and x represents either θ or q . However, in cold outbreaks, Chou and Atlas (1982), (hereafter referred to as I), developed a method based on the planetary boundary layer model of Stage and Businger (1981, a,b). They show that the vertical gradient in the bulk formula can be parameterized in terms of the downstream horizontal gradient. The resultant total heating of an air column over the distance of travel from the upwind shore is expressed by Eqs. (2) and (3) for sensible and latent heat.

$$S = \rho C_p u \int_0^{\infty} C_T (\theta_0 - \theta) dx \quad (2) \quad E = \rho L u \int_0^x C_q (q_0 - q) dx \quad (3)$$

Using the model of Stage and Businger, I showed that S and E are essentially linear with $(\theta_0 - \theta_1)$ and $(q_0 - q_1)$, respectively. Here θ_1 and q_1 are the values of θ and q at the upwind shore (or the upwind end) of the path. Thus, given these values, a measurement of the SST any place upstream of the cloud edge determines the sensible heating S . The presence of clouds invalidates the results thus constraining the method to the cloud-free region near shore. Similarly, since the SST determines the saturation mixing ratio at the sea surface, knowledge of q_1 at the shore determines the moisture and latent heat flux.

Fig. 1 is a nomogram for column sensible heating. The abscissa, labeled "cloud free distance" may be replaced simply by downstream distance provided it does not extend beyond the upstream edge of the clouds. There is a similar nomogram for latent heating. In order to convert the column heating to a flux one must multiply by the wind speed. Wind speed can be sensed remotely by one of the well known methods. Note that the sensitivity to downstream distance is small. For most realistic cases, the SST (θ_0) varies with fetch so that the SST implicitly includes the effect of distance. In any case, S may be estimated to better than $\pm 25\%$ independent of downstream distance.

2.2 Downstream Growth of Boundary Layer

One of the problems with the Chou-Atlas method is its dependence upon the lapse rate at the shore end. However, for accuracies of $\sim 10\%$ the lapse rate is not important. For greater accuracy they suggest that one use the downwind derivative of the square of the boundary layer depth Z_B as a proxy for lapse rate. This would be a convenient way if Z_B could be observed by lidar. As a good approximation for non-divergent conditions, we may write

$$dZ_B^2/dx \approx 2(1 + A_\theta)C_T(\theta_0 - \theta_1)/\Gamma_\theta \quad (4)$$

where A_θ is the entrainment coefficient, the ratio of the flux entrained across the PBL inversion to the surface flux. Eq. (4) is plotted in Fig. 2. As can be seen from Fig. 1 the column sensible heating is most sensitive to the temperature

contrast ($\theta_0 - \theta_1$). Accordingly, to a good approximation, the curves of ($\theta_0 - \theta_1$) in Fig. 2 may be replaced by isopleths of S. As a result, the quantity (dZ_B^2/dx) becomes a more direct measure of sensible heating. More precisely, following I

$$S = \rho C_p \chi^{-1} \int_0^x [0.5\Gamma_\theta / (1 + 2A_\theta)] [dZ_B^2/dx] dx \quad (5)$$

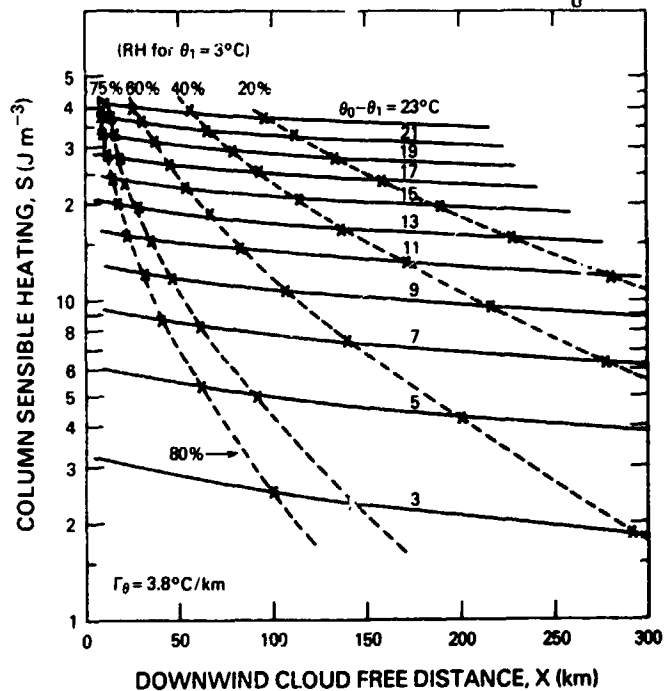


Fig. 1. Mean column sensible heating (S) between shore and downwind cloud free distance (x) versus x for various land air-sea surface temperature differences ($\theta_0 - \theta_1$) under non-divergent conditions and initial potential temperature lapse rate of $3.8^\circ\text{C km}^{-1}$ (solid lines). Dashed lines correspond to the cloud-free paths for various surface relative humidities (RH) and initial shore surface air temperature (θ_1) of 3°C . Each cross indicates a numerical experiment (after Chou and Atlas, 1982).

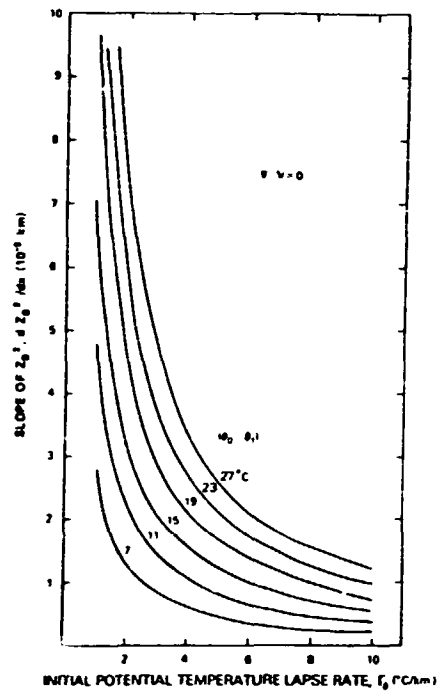


Fig. 2. Slope of Z_B^2 versus the initial potential temperature lapse rate (Γ_0) for various ($\theta_0 - \theta_1$) under non-divergent conditions. ($\theta_0 - \theta_1$) may be replaced approximately by S the column sensible heating.

Column sensible heating is thus directly proportional to the average values of (dZ_B^2/dx). We assume that Z_B is measured by lidar. Note that these results pertain to cloud-free regions.

2.3 The depth of the entrainment zone.

An interesting feature of the unstable marine boundary layer is the roughness at the inversion and the depth of penetration of the buoyant elements into the stable layer. Deardorff et al. (1980) have shown that these characteristics carry significant information.

Fig. 3 shows the structure of the clear air portion of a convective PBL observed by airborne lidar during a cold outbreak off the NE coast of the United States (Melfi et al., 1983). The convection is made visible by the sea salt aerosols. In this case, the turrets do not appear to grow with distance because the flight is parallel to

shore and the section is normal to the wind. The organized structure is remarkable. The turret tops correspond closely to the top of the inversion; the troughs to the bottom as shown in Fig. 4.

Following Deardorff et al. (1980), Melfi et al. (1983) have computed the parameters \bar{h} , h_0 , h_2 , and Δh as shown in Fig. 4. The quantity h_0 , corresponding to the altitude attained by more than 96% of the turrets, represents the top of the well mixed layer at the base of the density inversion; the height h_2 , attained by 4% of the turrets, is the top of the inversion. \bar{h} is the median height; Δh is the depth of the entrainment zone and the inversion. Melfi et al. (1983), show that

$$[(\bar{h}/h_0) - 1] = [(\omega'\theta')_{\bar{h}}/(\omega'\theta')_s] = A_0 \quad (6)$$

With lidar data of the quality shown in Fig. 3, it is now possible to compute the value of A_0 , rather than assume it.

Assuming zero divergence, one can set

$$dz_B/dx = \omega_e/\mu \quad (7)$$

where w_e is the entrainment velocity and u is the wind speed in the mixed layer. Melfi et al. (1983), analyzed the laboratory data of Deardorff et al. (1980), and showed that

$$(\Delta h/h_0) \approx 3(\omega_e/\omega_*)^{0.5} \quad (8)$$

If this laboratory experiment simulates the atmosphere, then lidar observations of $(\Delta h/h_0)$ and (dz_B/dx) should permit the estimation of both the entrainment velocity, w_e , and the turbulent vertical velocity scale w_* defined by

$$\omega_* = [(g/\bar{\theta})(\omega'\theta')_s \bar{h}]^{1/3} \quad (9)$$

We see that w_* is a function of the surface flux $(\omega'\theta')_s$ and the height \bar{h} . Clearly high resolution lidar observations tell us much about the unstable PBL and fluxes. Since both the lidar schemes assume zero divergence, the results should be considered only as approximations.

BOUNDARY LAYER LIDAR



Fig. 3. West-east vertical cross section of convective streets made visible to airborne down-looking lidar (0.53 μ m wavelength) by scatter from sea salt aerosols on January 20, 1983. It took 5.3 min to fly from left to right (after Melfi et al., 1983).

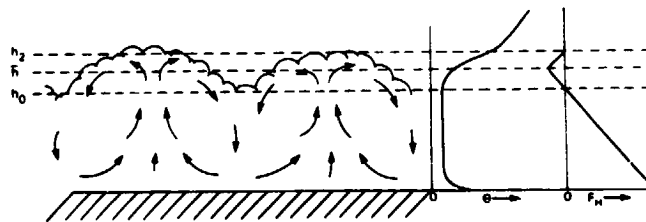


Fig. 4. Schematic showing the flow in the PBL and the vertical profiles of potential temperature and heat flux.; see text (after Melfi et al., 1983).

2.4 Measurements of water vapor (latent) heat flux.

The measurement of water vapor flux is done by measuring the vertical integrals of vapor at both the upwind and downwind ends of the path over the ocean; the difference is the integrated flux from below. Let the integrals over the column be Q_1 and Q_2 . The flux is then

$$F_q = \mu(Q_2 - Q_1)\lambda^{-1} \quad (10)$$

There are at least two basic schemes of measuring the total burden of water vapor (Q) in a beam extending from a satellite instrument to the surface. One operates in the IR; the other in the microwave band. Prabhakara et al. (1979) have used the 8 m to 9 m spectral window as observed by the Nimbus 4 Infrared Interferometer Spectrometer (IRIS) to measure the precipitable water over the oceans. They report an accuracy of about $\pm 15\%$ ($\sim 0.45 \text{ g cm}^{-2}$) rms and a measurement threshold of 1 g cm^{-2} as compared to radiosonde data. Prabhakara et al. (1982) have also shown that the difference in microwave brightness temperature between the 19 and 21 GHz channels on the Nimbus 7 Scanning Multichannel Microwave Radiometer (SMMR) also provides a measure of Q . The latter method yields an rms error of 0.25 g cm^{-2} and a threshold of about 0.5 g cm^{-2} . Gloersen et al. (1983) have used this approach to map the global distribution of mean seasonal integrated vapor

Recent developments have stimulated the move to the 183 GHz water vapor absorption line as a means of profiling water vapor radiometrically (Wang et al., 1983). Because of the strength of this line, it is believed that such a radiometer will provide especially high accuracy and an exceedingly small Q threshold. At this time, however, no quantitative estimates can be given.

For climatic purposes it is generally accepted that a precision of 10 to 15 watts m^{-2} would be useful over times of a few weeks to discern significant changes. To achieve a precision of 10 watts m^{-2} in the latent heat flux over a time of 10^4 sec. and over a corresponding path would require a precision of about $4 \times 10^{-3} \text{ g cm}^{-2}$ in the measured difference in Q . This can not be done with existing methods. However, it is thought to be attainable with the sensitive 183 GHz system (T. T. Wilheit, private communication). The smallest significant value of water vapor worthy of detection is about 0.2 g cm^{-2} . This is below the detection thresholds of either the present methods, but it is probably achievable in the 183 GHz band. By and large the effects of most clouds may be neglected. Only the large high liquid water content clouds will contaminate the measurements.

In the case of cold outbreaks within a few hundred kilometers from shore, one may assume that the air above the PBL is very dry. Accordingly, any downstream difference in the column integral of vapor is attributable to flux from the ocean. In other situations, however, it is possible that advection across the direction of the surface wind at levels above the PBL may contribute to the observed changes in Q . In the absence of a high resolution water vapor profiling system such as the DIAL lidar (Wilkerson and Schwemmer, 1983) it may be impossible to make the needed corrections. The only reasonable alternative is to use a regional or global circulation model (GCM) which incorporates a parameterization of surface fluxes and permits one to compute advective fluxes above the PBL. Of course, the accuracy of the model calculations is subject to question. However, one may assume that they provide acceptable approximations if they simulate the essential atmospheric features.

2.5 Inferring temperature profiles from cloud features.

Another set of schemes to approximate the flux in cold air outbreaks are illustrated in Fig. 5. Here, the basic idea is to deduce the change in the air column as it moves from near shore out over the ocean. This is what Henry and Thompson (1976) did over the Gulf of Mexico. But they used actual radiosonde data. In our case, there is no sounding available at the downwind end of the path. Accordingly, the sounding must be made by remote sensing methods.

For this purpose, one may use the upwind cloud edge position. We assume that all the changes in the temperature and humidity profiles occur in the PBL. Radiometric measurements may be made of the cloud top temperature near the upwind end of the cloud streets. Since the air in the PBL is well mixed, one assumes an adiabatic profile from the surface to the cloud top as in sounding B in Fig. 5. One can neglect the unstable profile in the immediate surface layer. The difference between the measured temperature profile at the shore and that deduced at the cloud edge is proportional to the total heat flux from the water. One can improve the accuracy by taking account of the entrainment across the inversion layer by increasing the estimate by about 20%. Henry and Thompson (1976) neglected this effect.

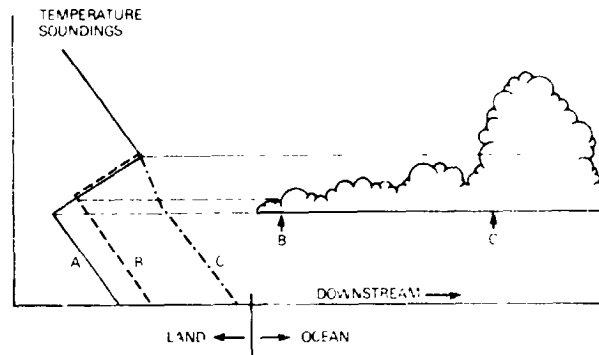


Fig. 5. Schematic of downstream growth of cloud streets in cold outbreak. Sounding A is measured at shore; B and C are inferred. B is near upwind cloud edge; C where clouds suddenly penetrate inversion.

A serious problem is that the clouds at the upwind end of the cloud streets do not usually fill the 1 km field-of-view of an instrument such as the TIROS-N Advanced Very High Resolution Radiometer (AVHRR). Hopefully, a future satellite will have better IR resolution. At present, the approach is usable only from aircraft. The resolution problem decreases as clouds grow larger downwind. But one then has to estimate the temperature profile assuming a wet adiabatic profile from cloud base to cloud top, and a dry adiabat in the PBL below cloud base. This requires knowledge of the cloud base height as obtainable from a model.

When the surface heating has produced a potential temperature in the PBL which exceeds the maximum temperature in the inversion, then the clouds will suddenly break through the inversion as shown at point C in Fig. 5. The downwind position of this event marks the point at which the equivalent potential temperature in the PBL is equal to that at the top of the inversion. The temperature profile there is then known at least approximately.

The latter approach assumes that there is no change in the temperature profile above the PBL from that measured at the shore line. Since this assumption is not always valid, the use of a lidar and a high resolution radiometer would provide the height and temperature coordinates from which soundings may be extrapolated downwards. We may assume that we have some measure of SST from prior measurements in clear air or from microwave observations. The SST provides an upper bound to the surface air temperature.

Our problems should be alleviated in the future through the use of lidar sounding techniques in the absence of clouds (Korb and Weng, 1982; Wilkerson and Schwemmer, 1982). Unlike passive methods, active sensors should be capable of giving vertical resolutions of 1 km for temperature and humidity from spacecraft and better resolution from aircraft. (Much higher resolution is achievable in measuring boundaries of clouds and aerosol layers.) The present spacecraft design studies consider instrument systems that require considerable time integration. This in turn, limits the horizontal spatial resolution to some 200 km. At this scale, the appearance of significant cloud cover anywhere along the path would contaminate the measurements. Unfortunately, we do not anticipate a lidar capability for the measurement of vertical profiles of temperature in the lowest few tens of meters.

2.6 Measurements of wind stress at sea surface.

For wind stress observations scatterometry has been proven to work under a range of wind conditions. However, work is needed to find optimal algorithms during cold outbreaks. Such conditions involve high winds, often above 20 m/s, and rapidly developing wave fields and boundary layers. Not only is there convective overturning in both the air and the water, but the mechanism of generation of turbulence in both media depend upon the waves, so that the mechanism is different from the turbulence generating process in the boundary layer of a rigid surface. This was reported by Donelan et al. (1983) and Kitaigorodskii (1983). One should therefore expect that one would have to take both the wave field and the wind into consideration when one attempts a parameterization of stress. Fortunately, under most conditions, the winds and the waves are related; thus a single parameter representation may be sufficient. But it may be inadequate under strongly developing waves where wind and waves are far from equilibrium, such as during cold outbreaks.

Breaking waves also create streamwise vorticity in the water, and the orbital velocity field of the waves stretch and compress this vorticity, causing turbulence production through vortex breakdown and shear instability. The measurements of Cavalieri under cold outbreak conditions in the Northern Adriatic (personal communication) shows that the shear stresses in the water can reach five to ten times the value given by conventional parameterizations based on wind speed.

Added to this is the fact that waves carry momentum. So the wind stress on the water surface will be found partly in the mean velocity field in the water boundary layer and partly in the wave field. Waves transport momentum at group velocity, so that momentum introduced into the water by wind stress can be converted to mean current far away from where the stress was put in. Scatterometry may still be a good method for measuring wind stress, since the short waves that the scatterometer observes are generated locally, although, of course, they may be affected by wave breaking and water turbulence.

2.7 Possible inferences of ocean effects.

Cold outbreaks cause cooling of the water, equal in heat to the heating of the atmosphere, and the overturning may reach to great depths. Horizontal variations in cooling lead to mean density gradients and thus to currents. After a particularly cold winter the effects may be dramatic; for example, after the winter of 1976-77 in the eastern U.S., Worthington (1977) showed that the speed of the Gulf Stream had reached an all time high.

However, few of the oceanographic consequences of cold outbreaks will be observable from satellites. It is therefore especially important to make the most out of the atmospheric observations so that one can relate total heat transfer, total evaporation and wind stress to changes in oceanic stratification and excitation of oceanic motions. This will have to be done through numerical modeling.

3. CONCLUDING REMARKS

We have attempted to gather a variety of concepts for the measurement or inference of the energy and vapor fluxes across the air-sea interface under conditions of unstable cold outbreaks. These proposed methods are summarized in the abstract. By and large, the techniques permit us to infer fluxes through the observation of the effects of the transports on the atmosphere such as the progressive downstream heating, moistening, and growth of the planetary boundary layer and associated cloud formation. The observed evolution of the PBL is related to the fluxes through the use of numerical and analytical models. The measurables include surface wind speed, SST, the downstream slope of the PBL as observed by lidar, the roughness and depth of the PBL inversion also observed by lidar, and precipitable water vapor as observed by either IR or microwave radiometry.

None of the concepts has been demonstrated and so the paper is necessarily speculative. Individually, the methods are subject to serious constraints; as a group, however, they complement each other and appear promising in providing reasonable estimates of the fluxes of heat and vapor.

4. ACKNOWLEDGEMENTS

The authors are indebted to Drs. S. H. Chou, S. H. Melfi, P. Cuddapah, T. T. Wilheit, and P. Gloersen for valuable discussions and the use of data from their papers. We also greatly appreciate the insight provided by Dr. Mark Helfand and the general assistance of Mr. Earl Kreins and Mrs. Tracy Pepin. All are members of our Laboratory.

5. REFERENCES

Chou, S. H. and D. Atlas, 1982: Satellite estimates of ocean-air heat fluxes during cold air outbreaks. *Mon. Wea. Rev.*, 110, 1434-1450.

Deardorff, J. W., G. E. Willis, and B. H. Stockton, 1980: Laboratory studies of the entrainment zone of a convectively mixed layer, *J. Fluid Mech.*, 100, 41 pp.

Donelan, M. A., S. A. Kitaigorodskii, J. L. Lumley, and E. A. Terray, 1983: A case study of wave-turbulence interactions in the marine surface layer. Talk given at the Sixth Symposium on Turbulence and Diffusion of American Meteorological Society, March 22-25, 1983.

Gautier, C., 1981: Proc. Workshop of Applications of Existing Satellite Data to the Study of the Ocean Surface Energetics, 19-21 November 1980. Rep. NASW-57380, University of Wisconsin Press, Madison, 237 pp.

Gloersen, P., D. J. Cavalieri, A. T. C. Chang, T. T. Wilheit, W. J. Campbell, K. F. Kunzi, R. O. Ramseier, D. B. Ross, D. Staelin, E. P. L. Windsor, F. T. Barath, P. Gudmandsen, O. M. Johannesen and E. Langham, (1984): A summary of results from the first Nimbus 7 SMMR observations. *J. Geophys. Res.* (in press).

ORIGINAL PAGE IS
OF POOR QUALITY

Henry, W. K. and A. H. Thompson, 1976: An example of polar air modification over the Gulf of Mexico. *Mon. Wea. Rev.*, 104, 1324-1327.

Kitaigorodskii, S. A., 1983: The equilibrium range in the spectrum of wind generated waves. Talk given at Sixth Symposium on Turbulence and Diffusion of American Meteorological Society, March 22-25, 1983.

Korb, C. L. and C. Y. Weng, 1982: A theoretical study of a two wavelength lidar technique for the measurement of atmospheric temperature profiles. *J. Appl. Meteor.*, 21, 1346-1355.

Melfi, S. H., J. D. Spinhirne, S. H. Chou, and S. Palm, 1983: Lidar observations of vertically organized convection in the planetary boundary layer over the ocean. *J. Clim. Appl. Meteor.* (to be submitted).

Prabhakara, C., H. D. Chang, and A. T. C. Chang, 1982: Remote sensing of precipitable water over the oceans from Nimbus 7 microwave measurements. *J. Appl. Meteor.*, 21, 59-68.

Prabhakara, C., G. Dalu, R. C. Lo, and N. R. Nath, 1979: Remote sensing of seasonal distribution of precipitable water vapor over the oceans and the inference of boundary-layer structure. *Mon. Wea. Rev.*, 107, 1388-1401.

Sanders, F. and J. R. Gyakum, 1980: Synoptic-dynamic climatology of the "bomb". *Mon. Wea. Rev.*, 108, 1589-1606.

Stage, S. A. and J. A. Businger, 1981a: A model for entrainment into a cloud-topped marine boundary layer -- Part I: Model description and application to a cold air outbreak episode. *J. Atmos. Sci.*, 38, 2213-2229.

Stage, S. A. and J. A. Businger, 1981b: A model for entrainment into a cloud-topped marine boundary layer -- Part II: Discussion of model behavior and comparison with other models. *J. Atmos. Sci.*, 38, 2230-2242.

Wang, J. R., J. L. King, T. T. Wilheit, G. Szejwach, L. H. Gesell, R. A. Nieman, D. S. Niver, B. M. Krupp, and J. A. Gagliano, 1983: Profiling atmospheric water vapor by microwave radiometry. *J. Appl. Meteor.*, 22, 779-788.

Wilkerson, T. D. and G. K. Schwemmer, 1982: Lidar techniques for humidity and temperature measurements, *Opt. Eng.*, 21, 1022-1024.

Worthington, L. V., 1977: Intensification of the Gulf Stream after the winter of 1976-77. *Nature*, 270, 415-417.